# Model Predictive Control for Transparent Teleoperation Under Communication Time Delay

Shahin Sirouspour, *Member, IEEE*, and Ali Shahdi, *Student Member, IEEE*

***Abstract*—Prior efforts in bilateral teleoperation under communication delay have mainly yielded control algorithms that sacrifice performance in order to guarantee robust stability. In contrast, this paper proposes a multimodel predictive controller that can enhance the teleoperation transparency in the presence of a known constant delay. Separate controllers are designed for free motion/soft contact and contact with rigid environments, with switching between these mode-based control laws occurring according to the identified contact mode. Performance objectives such as position tracking and tool impedance shaping for free motion/soft contact, as well as position and force tracking for contact with rigid environments, are incorporated into a multi-input/multi-output state-space representation of the system dynamics. New Artstein-type state and measurement transformations are proposed to generate delay-free dynamics suitable for output-feedback control, based on the original dynamics with delays in various input and output channels. The application of the continuous-time linear quadratic Gaussian control synthesis to the resulting mode-based delay-free dynamics yields control laws that guarantee closed-loop stability and enhanced performance in each phase of teleoperation. The robustness of the mode-based controllers with respect to parametric uncertainty is analyzed. Experimental results with a single-axis teleoperation setup demonstrate the effectiveness of the proposed approach.**

***Index Terms*—Delay reduction, linear quadratic Gaussian (LQG) control, multimodel control, teleoperation, telerobotics, time delay, transparency.**

## I. Introduction

TELEOPERATION systems allow a person to extend his/her intelligence and manipulation skills to remote and/or hazardous environments through coordinated control of two robotic arms, i.e., a master hand controller used by the operator, and a slave robot that manipulates the environment. Applications of teleoperation are numerous, ranging from space operation, underwater exploration, and mining, to nuclear material handling, toxic material handling, and robotic-assisted medical interventions [1], [2]. In unilateral teleoperators, the master position and/or force data are transmitted to the slave site, while only visual information from the task environment is sent back to the operator. In bilateral teleoperation, however, position/force data are communicated in both directions between master and slave. By providing haptic and kinesthetic feedback, bilateral teleoperators can facilitate task execution through the establishment of a virtual presence in the task environment, an objective denoted as transparency in the literature [3].

Several teleoperation control architectures have been proposed in the literature that employ bidirectional flow of force and position information between the master and slave. These include position–position [4], position–force [5], [6], force–force [7], and the four-channel [3], [8] teleoperation approaches. Linear controllers based on the $\mu$-synthesis and $H_\infty$ theories have been developed to achieve robust stability and enhanced performance in the presence of uncertainties in the system dynamics [6], [9]–[11]. In [12], local master/slave adaptive nonlinear position/force controllers have been combined with teleoperation coordinating controllers to guarantee stable teleoperation in the presence of dynamic uncertainty. Based on the concept of passive decomposition, the authors in [13] propose a nonlinear controller that can provide useful task-specific dynamics for inertia scaling, motion guidance, and obstacle avoidance. A time-domain passivity-based controller has been proposed in [14] for teleoperation under a wide variety of environments and operating speeds.

Data transmission delay in teleoperation can be anywhere from less than a millisecond to several minutes, depending on the distance between the master and slave sites and the medium of communication. In the control design, this latency imposes a tradeoff between the conflicting requirements of stability and performance with the potential for instability increasing by the level of the performance. In [15], a rigorous analysis of the robust stability of a few bilateral teleoperation architectures with respect to (w.r.t.) time delay is presented. In [16], some existing teleoperation control schemes that address the issue of time latency are compared from the stability and performance perspectives.

Although by adding sufficient damping at the master and slave ends, a delayed bilateral teleoperation system can be stabilized, e.g., see [17], such an approach would often result in a very sluggish response. Also, the scattering theory and the concept of passivity have been widely employed to guarantee stable teleoperation, irrespective of the amount of time delay, in [18]–[22], among other references. Nevertheless, the performance of these methods is notably compromised in favor of their robust stability. In [23], an adaptation of line-terminating impedance functions is proposed to remedy the loss of transparency in bilateral teleoperation, based on the scattering theory. In [24], the concept of telemonitoring force feedback for teleoperation under short time delays is introduced. Used

Manuscript received December 9, 2005; revised May 8, 2006. This paper was recommended for publication by Associate Editor P. Rocco and Editor H. Arai upon evaluation of the reviewers' comments. This work was supported in part by the Natural Sciences and Engineering Research Council of Canada, in part by the Canada Foundation for Innovation, and in part by the Ontario Innovation Trust. Color versions of Figs. 4-10 are available online at http://ieeexplore.org.

The authors are with the Department of Electrical and Computer Engineering, McMaster University, Hamilton, ON L8S 4K1, Canada (e-mail: sirouspour@ece.mcmaster.ca; shahdisa@mcmaster.ca).

Digital Object Identifier 10.1109/TRO.2006.882939

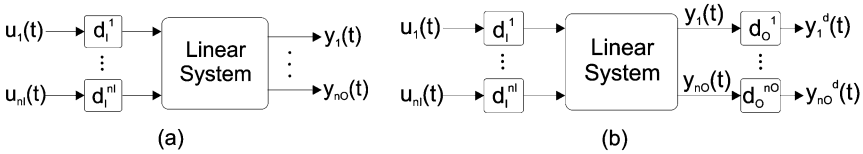


Fig. 1. Linear system with (a) delayed control actions and (b) delayed control actions and delayed measurements.

for teleoperation under long delays up to several seconds, predictive display-based controllers rely on accurate models of the task environment to provide the operator with a realistic delay-free simulated response of the remote manipulator and environment [25], [26]. Predictive control methods such as the Smith predictor have also been developed for teleoperation [16], [27]. In [27], the wave-based teleoperation controller is combined with a Smith predictor, a Kalman filter, and an energy regulator to improve its transparency. Finally, in [28], the authors have employed a first-order Taylor approximation to time delay in a state-space approach to the teleoperation control.

This paper follows upon the authors' earlier work in [29], in which a discrete-time linear quadratic Gaussian (LQG) controller for teleoperation under communication time delay was proposed. In that paper, the time delay was incorporated into a finite-dimension state-space model of the system in the discrete-time domain. One drawback of this approach is that the number of system states is proportional to the delay and the control rate. Therefore, to reduce the computational load and avoid potential numerical problems, the sampling rate must be limited as the delay increases. This may not be desirable, since a low sampling rate can negatively impact the closed-loop response and stability of teleoperation.

There has been considerable effort in the stability analysis and control synthesis for the time-delay systems, and the interested reader is referred to the survey papers on this topic in [30] and [31]. Kwon *et al.* [32] and later Artstein [33] introduced transformations to reduce an infinite-dimensional continuous-time linear control system with delayed control actions to an equivalent control system without delay. In this paper, this method has been revised such that it can be applied to systems with different delays in various control and measurement channels. This modified reduction technique is then used to produce a delay-free variation of the teleoperation system dynamics. An LQG observer/controller pair is synthesized to achieve the transparency objectives using position and force measurements at the master and slave sides. The latency is assumed to be *a priori* known constant. The environment dynamics can vary widely in a teleoperation task, and introduce significant uncertainty into the system model. To mitigate this problem, multiple controllers along with proper switching rules are employed for different phases of teleoperation. Such an adaptive control approach is less conservative, and can potentially yield superior performance over single-mode controllers.

In summary, the major contributions of this paper are: 1) A novel approach to the reduction and output-feedback control of multi-input/multi-output (MIMO) systems with nonidentical delays in various input and output channels is proposed. It is proven that the reduced system inherits the detectability and stabilizability properties of the original system. Also, it is shown that the closed-loop stability of the reduced system implies the stability of the original system; 2) teleoperation under time delay is formulated as a multimodel continuous-time LQG synthesis problem using the proposed output-feedback control approach. The performance indices used include nondelayed position tracking, force tracking, and virtual-tool impedance shaping.

The rest of this paper is organized as follows. The output-feedback control for delayed MIMO systems is discussed in Section II. Dynamics of a bilateral teleoperation system are introduced in Section III. The LQG teleoperation control synthesis is discussed in Section IV. In Section V, a robust stability analysis is presented for a single-axis teleoperation design example. Experimental results are given in Section VI. The paper is concluded in Section VII.

## II. Delayed System Reduction and Control

In [33], Artstein introduced a transformation to reduce an infinite-dimensional system with delays in control actions to a delay-free system. Consider the MIMO linear delay system shown in Fig. 1(a) with the following state-space dynamics:

$$\dot{X}(t) = AX(t) + \sum_{j=1}^{n_I} B_j u_j(t - d_I^j) + Gw(t) \tag{1}$$

$$y_k(t) = C_k X(t) + \sum_{j=1}^{n_I} D_{kj} u_j(t - d_I^j) + H_k w(t) + \upsilon_k(t), \quad k = 1, \ldots, n_O \tag{2}$$

where $X(t)$ is the vector of states, $y_k(t)$ is the $k$th output vector, and $u_j(t)$ is the $j$th input vector; $n_I$ and $n_O$ are the numbers of inputs and outputs, respectively; $d_I^j$ is the delay in the $j$th input channel; $w(t)$ and $\upsilon_k(t)$ are process and measurement noise, respectively; and $A, B, C, D, G$, and $H$ are constant matrices with proper dimension. By taking the derivative of a new state $Z(t)$ defined as

$$Z(t) = X(t) + \sum_{j=1}^{n_I} \int_{t-d_I^j}^{t} e^{A(t-s-d_I^j)} B_j u_j(s) ds \tag{3}$$

and substituting $\dot{X}(t)$ from (1), one may write

$$\dot{Z}(t) = AZ(t) + \sum_{j=1}^{n_I} e^{-Ad_I^j} B_j u_j(t) + Gw(t). \tag{4}$$

The new system in (4) has no delay in its control signals, and therefore, a state-feedback can be implemented for its stabilization. The optimal linear quadratic (LQ) output-feedback control of input-delayed systems using such transformations has also been addressed in [34]. Note that systems with delays in both

input and output channels can simply be converted to an equivalent system with delays in inputs, if the delays in all output or all input ports are equal. However, for reasons that will become clear later in the paper, teleoperation control systems involve nonidentical delays in their input and output channels, as shown in Fig. 1(b) for a generic system. Since the existing delay-reduction techniques is not directly applicable to such systems, in this paper, a revised state/measurement transformation is proposed to address this problem. Due to the presence of delay in the output channels, (2) is rewritten as

$$\begin{aligned} y_k^d(t) &= y_k\left(t-d_O^k\right) \\ &= C_kX\left(t-d_O^k\right)+\sum_{j=1}^{n_I}D_{kj}u_j\left(t-h_j^k\right) \\ &\quad + H_kw\left(t-d_O^k\right)+\upsilon_k\left(t-d_O^k\right) \end{aligned} \tag{5}$$

where $w(t)$ and $\upsilon_k(t)$ are defined in (2), $d_O^k$ is the delay in the $k$th output channel, and $h_j^k$ is the total delay between $j$th input and $k$th output, i.e., $h_j^k \triangleq d_I^j + d_O^k$. A revised state transformation is defined as

$$Z(t) = X\left(t-d_O^m\right)+W_m(t) \tag{6}$$

where $d_O^m = \max\{d_o^i\}, i=1,\ldots,n_O$ is the maximum latency in measurement channels, and

$$W_k(t) = \sum_{j=1}^{n_I}\int_{t-h_j^k}^{t} e^{A(t-s-h_j^k)}B_ju_j(s)ds. \tag{7}$$

Taking the time derivative of (6) and replacing $\dot{X}(t-d_O^k)$ from (1) yields

$$\dot{Z}(t) = A_zZ(t)+B_zu(t)+Gw\left(t-d_O^m\right) \tag{8}$$

with

$$A_z = A, \quad B_z = \left[e^{-Ah_1^m}B_1 \quad \cdots \quad e^{-Ah_{n_I}^m}B_{n_I}\right]. \tag{9}$$

For the system described in (1), $X(t-d_O^m)$ can be written in terms of $X(t-d_O^k)$ using standard results from the linear systems theory as follows [35]:

$$\begin{aligned} &X\left(t-d_O^m\right) \\ &\quad = e^{-Ad_O^{mk}}X\left(t-d_O^k\right)-\sum_{j=1}^{n_I}\int_{t-h_j^m}^{t-h_j^k}e^{A\left(t-s-h_j^m\right)} \\ &\qquad \times B_ju_j(s)ds-\int_0^{d_o^{mk}}e^{-As}Gw\left(t-d_o^m+s\right)ds \end{aligned} \tag{10}$$

where $d_O^{mk} = d_O^m - d_O^k$. Replacing $X(t-d_O^m)$ in (6) from (10) results in

$$\begin{aligned} Z(t) &= e^{-Ad_O^{mk}}X\left(t-d_O^k\right)+\sum_{j=1}^{n_I}\int_{t-h_j^k}^{t}e^{A\left(t-s-h_j^m\right)}B_ju_j(s)ds \\ &\quad -\int_0^{d_o^{mk}}e^{-As}Gw\left(t-d_o^m+s\right)ds \end{aligned} \tag{11}$$

and by multiplying both sides from left by $C_ke^{Ad_o^{mk}}$ and substituting $C_kX(t-d_o^k)$ from (5), one may write

$$\begin{aligned} &C_ke^{Ad_o^{mk}}Z(t) \\ &\quad = y_k^d(t)-\sum_{j=1}^{n_I}D_{kj}u_j\left(t-h_j^k\right)-H_kw\left(t-d_O^k\right) \\ &\qquad -C_k\int_{-d_o^{mk}}^{0}e^{-As}Gw(t+s)ds-\upsilon_k\left(t-d_O^k\right) \\ &\qquad +C_kW_k(t). \end{aligned} \tag{12}$$

A new output vector for the $k$th channel, $y_z^k(t)$, is defined as

$$\begin{aligned} y_z^k(t) &= C_ke^{Ad_o^{mk}}Z(t)+H_kw\left(t-d_O^k\right) \\ &\quad +\upsilon_k\left(t-d_O^k\right)+C_k\int_{-d_o^{mk}}^{0}e^{-As}Gw(t+s)ds. \end{aligned} \tag{13}$$

By stacking the new output vectors, one can write

$$y_z(t) = C_zZ(t)+\upsilon_z(t) \tag{14}$$

with $C_z = [(C_1e^{Ad_o^{m1}})^T\ (C_2e^{Ad_o^{m2}})^T\ \cdots\ (C_{no}e^{Ad_o^{mn_o}})^T]^T$ and

$$\begin{aligned} \upsilon_z^k(t) &= H_kw\left(t-d_o^k\right)+\upsilon_k\left(t-d_o^k\right) \\ &\quad +C_k\int_{-d_o^{mk}}^{0}e^{-As}Gw(t+s)\,ds. \end{aligned} \tag{15}$$

Using (12), the reduced system outputs in (13) can be calculated from the actual delayed outputs and $W$'s using

$$y_z^k(t) = y_k^d(t)-\sum_{j=1}^{n_I}D_{kj}u_j\left(t-h_j^k\right)+C_kW_k(t). \tag{16}$$

This completes the derivation of the reduced system dynamics and the output equations in (8) and (14). The calculation of the new observation vectors in (16) involves the computation of $W_k(t)$'s in (7) which are outputs of systems with finite impulse response (FIR). Alternatively, $W_k(t)$'s and the transformed outputs can be computed as follows

$$\begin{aligned} \dot{W}_k(t) &= AW_k(t)+\sum_{j=1}^{n_I}e^{-Ah_j^k}B_ju_j(t)-\sum_{j=1}^{n_I}B_ju_j\left(t-h_j^k\right) \\ y_k^w(t) &= C_kW_k(t). \end{aligned} \tag{17}$$

Since the states of the system are unavailable, an observer/controller pair must be designed to control the reduced system based on the new output measurements. The following theorem is needed in the control of the reduced system.

*Theorem 2.1:* The reduced system in (8) and (14) is stabilizable and detectable if the original system in (1) and (2) is stabilizable and detectable.

*Proof:* See the Appendix.

The LQG control synthesis can now be applied to the reduced system in (8) and (14) which is perturbed by the disturbance and noise signals $w(t-d_O^m)$ and $\upsilon_z(t)$. It should be noted that these stochastic inputs do not satisfy the optimality conditions of the LQG control, i.e., being white Gaussian and uncorrelated. In fact, in practice, it is hard to find a system that can satisfy the optimality conditions on disturbance and noise signals. It is even harder to establish the optimality of a switching control

strategy such as the one used in this paper. However, the stability results obtained from the LQG synthesis do still apply for the mode-based controllers.

The LQG controller attempts to minimize the effect of the stochastic disturbance inputs on the states through minimizing the following cost function as $T \to \infty$ [36]:

$$J(u) = \frac{1}{T} E\left\{ \int_0^T [Z(t)^T Q Z(t) + u(t)^T R u(t)] dt \right\} \quad (18)$$

where $E\{\cdot\}$ denotes the expected value, and $Q \geq 0, R > 0$. The optimal controller is a combination of a constant state-feedback gain obtained from solving the corresponding deterministic optimal LQ control and an optimal Kalman filter state estimator, i.e.,

$$u(t) = -K\hat{Z}(t), \quad K = R^{-1}B^T S \quad (19)$$

where $S$ is the solution to the following continuous-time algebraic Riccati equation (CARE):

$$A^T S + SA - SBR^{-1}B^T S + Q = 0. \quad (20)$$

The state estimate $\hat{Z}(t)$ is the output of a Kalman filter with the following dynamics:

$$\dot{\hat{Z}}(t) = A\hat{Z}(t) + Bu(t) + L[y_z(t) - C\hat{Z}(t) - Du(t)]. \quad (21)$$

The Kalman filter gain $L$ is computed as follows:

$$L = PC^T \Pi^{-1} \quad (22)$$

and $P$ is the solution to the following CARE:

$$PA^T - PC^T \Pi^{-1} CP + AP + W = 0 \quad (23)$$

with $W = E\{Gw(t)w(t)^T G^T\}$ and $\Pi = E\{\upsilon_z(t)\upsilon_z(t)^T\}$ being the covariances of the process and measurement noise, respectively. Certain conditions must be satisfied for the existence of a solution to the LQG problem. These include the stabilizability of pair $(A, B)$ and detectability of pair $(C, A)$, among others. It can be shown that the teleoperation system satisfies all necessary requirements. Furthermore, in *Theorem 2.1*, it is proven that the stabilizability and detectability are preserved under the proposed state and output transformations.

*Theorem 2.2:* If the reduced delay-free system is stabilized through an observer/controller pair, the original delayed system will also become stable.

*Proof:* The stability of the reduced system/observer implies that the reduced states $Z(t)$ and their estimates $\hat{Z}(t)$ remain bounded in the presence of bounded disturbance and noise. Hence, the control signal $u(t)$ which is given by (19) is also bounded. From (6), the original system states can be written as

$$X\left(t - d_O^m\right) = Z(t) - W_m(t) \quad (24)$$


Fig. 2. Teleoperation control of a robot.

where

$$W_m(t) = \sum_{j=1}^{n_I} \int_{t-h_j^m}^{t} e^{A\left(t-s-h_j^m\right)} B_j u_j(s) ds \quad (25)$$

and $W_m(t)$ is bounded as a result of the boundedness of $u(t)$. Since both terms on the right-hand side (RHS) of (24) are bounded, $X(t - d_O^m)$ and consequently $X(t)$ are also bounded. Therefore, the pair of observer/controllers for the delay-free reduced system stabilizes the original system, as well. Note that if zero is an asymptotically stable point for the reduced states $Z(t)$, then it would also be an asymptotically stable point for the original states $X(t)$. Q.E.D.

## III. Modeling and Dynamics of Teleoperation Systems

Five distinct elements constitute a bilateral teleoperation system, as shown in Fig. 2. These are the human operator, master robot, controllers and communication channel, slave robot, and the environment [37]. The haptic interfaces employed in teleoperation are generally rigid multibody mechanical devices with second-order nonlinear dynamics, as follows:

$$D(X)\ddot{X} + C(X, \dot{X})\dot{X} + G(X) = F_h + F_{\text{cm}}^n \quad (26)$$

where $X \in \mathbb{R}^6$ is a generalized position vector of the device, $F_h \in \mathbb{R}^6$ is a generalized vector of hand forces, $F_{\text{cm}}^n \in \mathbb{R}^6$ is a vector of control signals, $D(X)$ is the inertia matrix, $C(X, \dot{X})\dot{X}$ contains Coriolis and centrifugal terms, and $G$ is the gravity vector. The robot dynamics in (26) can be written in a linear-in-parameter format as follows [38]:

$$D(X)\ddot{X} + C(X, \dot{X}_1)\dot{X}_2 + G(X) = Y(\ddot{X}, \dot{X}_1, \dot{X}_2, X)\theta \quad (27)$$

where $Y(\cdot)$ is a regressor matrix, and $\theta$ is a vector of unknown parameters.

*Theorem 3.1:* Consider the robot dynamics in (26) and the control law

$$F_{\text{cm}}^n = -F_h + Y(\ddot{X}_r, \dot{X}, \dot{X}_r, X)\hat{\theta} - K_d\rho \quad (28)$$

with

$$\dot{X}_r = \dot{X}_d - \Lambda\tilde{X}, \quad \tilde{X} = X - X_d, \quad \rho = \dot{\tilde{X}} + \Lambda\tilde{X}$$
$$X_d = X - L^{-1}\{(s^2M + sB + K)^{-1}(F_h + F_{\text{cm}})\} \quad (29)$$

where $L^{-1}\{\cdot\}$ is the inverse Laplace transform, $s$ is the Laplace variable, $K_d > 0, \hat{\theta}$ is a parameter estimate, and the parameter adaption law

$$\dot{\hat{\theta}}_i = \begin{cases} 0, & \text{if } -[\Gamma Y^T \rho]_i > 0, \quad \theta_i > \theta_i^{\max} \\ 0, & \text{if } -[\Gamma Y^T \rho]_i < 0, \quad \theta_i < \theta_i^{\min} \\ -[\Gamma Y^T \rho]_i, & \text{otherwise} \end{cases} \tag{30}$$

with $\Gamma > 0, [\cdot]_i$ denotes the $i$th element of the argument vector, and $\theta_i^{\min}$ and $\theta_i^{\max}$ are *a priori* known lower and upper bounds on the individual unknown parameters. Then, the resulting closed-loop dynamics are governed by

$$M\ddot{\bar{X}} + B\dot{\bar{X}} + K\bar{X} = \bar{F}_h + \bar{F}_{\rm cm} + \eta \tag{31}$$

where $\eta \in L_2 \cap L_\infty$ and $\bar{X}, \bar{F}_h$, and $\bar{F}_{\rm cm}$ are produced by passing the corresponding variables through a linear lowpass filter with transfer function $H(s) = c/(s+c)$.

*Proof:* Following steps similar to those in [39], we define the Lyapunov function

$$V(t) = \frac{1}{2}\rho^T D(X)\rho + \frac{1}{2}\tilde{\theta}^T \Gamma^{-1}\tilde{\theta} \tag{32}$$

where $\tilde{\theta} = \hat{\theta} - \theta$ is the parameter estimation error. By taking the derivative of $V(t)$ and using the control and adaption laws in (28)–(30), as well as the skew-symmetry property of $\dot{D} - 2C$, it can be shown that

$$\dot{V}(t) \le -\rho^T K_d \rho. \tag{33}$$

By considering (32) and (33), one can conclude that $\rho \in L_\infty$. Also, an integration of (33) shows $\rho \in L_2$. Consequently, $\tilde{X}, \dot{\tilde{X}} \in L_2 \cap L_\infty$ and $\tilde{X} \to 0$. Now using the definition of $\tilde{X}$ and $X_d$ in (29), it is straightforward to show that (31) holds with

$$\eta = L^{-1}\left\{(s^2 M + sB + K)\frac{c}{s+c}\tilde{X}(s)\right\}. \tag{34}$$

Given that $\tilde{X}, \dot{\tilde{X}} \in L_2 \cap L_\infty$, it can be concluded that $\eta \in L_2 \cap L_\infty$. The disturbance $\eta$ to the linearized dynamics in (31) can be handled by the LQG design framework presented earlier in the paper. It is worth noticing that the implementation of the nonlinear control law in (28) requires position, velocity, and force signals, as well as $\dot{\bar{F}}_{\rm cm}$. The first three signals are available through sensors, while the last signal can be calculated from $-K\dot{\hat{Z}}(t)$ according to (19). The derivative of the reduced state estimate $\dot{\hat{Z}}(t)$ can be obtained from the Kalman filter in (21). As will be seen in Section IV, the application of the LQG controller to the filtered dynamics in (31) will guarantee position tracking, virtual intervening tool impedance shaping, as well as force tracking of the filtered master and slave variables. Therefore, the performance objectives will be achieved for a frequency range determined by the bandwidth of the first-order filter $H(s)$. Obviously, if the robot dynamics are linear and known, as will be in the case of our experimental setup, the original dynamics can be directly employed in the LQG synthesis.

In general, the dynamics of the slave robot are similar to those of the master robot, i.e., second-order and nonlinear. These dynamics can also be linearized through the application of local dynamic-feedback-linearizing control laws. Throughout the rest of this paper, without loss of generality, we assume the linearized master/slave dynamics are decoupled in different axes of motion. Hence, we only treat a single-axis teleoperation problem, though the approach can be extended to a multivariable case.

The linearized single-axis master dynamics are governed by

$$m_m\ddot{x}_m + b_m\dot{x}_m + k_m x_m = f_{\rm cm} + f_h \tag{35}$$

where $m_m, b_m$, and $k_m$ are mass, damping, and stiffness of the master interface, and $x_m$ is its position; $f_{\rm cm}$ is the control signal; and $f_h$ is the operator/device interaction force. The operator's arm dynamics are approximated by a second-order linear time-invariant differential equation

$$m_h\ddot{x}_m + b_h\dot{x}_m + k_h x_m = f_h^* - f_h \tag{36}$$

where $m_h, b_h$, and $k_h$ are mass, damping, and stiffness of the operator's arm, respectively; $x_m$ has been defined in (35); $f_h^*$ is the operator's intentional force and is modeled as an exogenous input to the system. This is in addition to the arm's dynamic reaction force, which is a function of the master motion variables. In general, dynamics of the arm are nonlinear, time-dependent, and posture-dependent. However, linear models have been successfully employed by previous researchers in their work [12], [40], and are adopted here as well. The arm dynamics in (36) can be incorporated into the master dynamics in (35) as follows:

$$(m_m + m_h)\ddot{x}_m + (b_m + b_h)\dot{x}_m + (k_m + k_h)x_m = f_{\rm cm} + f_h^*. \tag{37}$$

The combined master and arm linearized dynamics can be easily written in the state-space form by selecting position and velocity as the state variables. The resulting equations will not be presented here for brevity.

The linearized dynamics of the slave are governed by

$$m_s\ddot{x}_s + b_s\dot{x}_s + k_s x_s = f_{\rm cs} - f_e \tag{38}$$

where $x_s$ is the position of the slave; $m_s, b_s$, and $k_s$ are the slave mass, damping, and stiffness, respectively; $f_{\rm cs}$ is the control signal; and $f_e$ is the environment reaction force. The reaction force for compliant environments can be modeled by

$$f_e = \begin{cases} m_e\ddot{x}_s + b_e\dot{x}_s + k_e x_s + f_e^*, & \text{in contact} \\ 0, & \text{free motion} \end{cases} \tag{39}$$

and $f_e^*$ is the exogenous environment force. This can be combined with the slave dynamics in (38) to obtain

$$(m_s + \sigma_f m_e)\ddot{x}_s + (b_s + \sigma_f b_e)\dot{x}_s + (k_s + \sigma_f k_e)x_s = f_{\rm cs} - \sigma_f f_e^* \tag{40}$$

where

$$\sigma_f = \begin{cases} 1, & \text{slave in contact} \\ 0, & \text{slave in free motion.} \end{cases} \tag{41}$$

Contact with a rigid environment can be modeled as [12]

$$m_s(1-\sigma_r)\ddot{x}_s + b_s(1-\sigma_r)\dot{x}_s + k_s x_s = f_{\rm cs} - \sigma_r f_e \quad (42)$$
$$\dot{x}_s = (1-\sigma_r)\dot{x}_s, \quad \ddot{x}_s = (1-\sigma_r)\ddot{x}_s \quad (43)$$

where $\sigma_r$ is similarly defined as in (41). Therefore, during a rigid contact, the slave acceleration and velocity are zero, and the environment force is equal to the slave control action less the stiffness force. By choosing $x_s$ and $\dot{x}_s$ as the state variables, the state-space representation of the combined slave/environment dynamics can be also obtained.

## IV. LQG Teleoperation Control

The performance of conventional single-master/single-slave telerobotic systems is measured by their transparency. In an ideally transparent telerobotic system, the operator should feel that he/she is directly interacting with the environment. This notion of transparency, also denoted as ideal kinesthetic coupling [8], can be expressed in terms of position and force tracking between the master and slave robots [8], [37]. Achieving ideal transparency requires acceleration, or equivalently, force measurement, and the exact knowledge of the master and slave dynamics. Moreover, in a perfectly transparent system, modeling errors can easily cause instability [8]. By including a virtual intervening tool between the operator and the task environment, a variant of transparency can be defined that eliminates these problems [8], [37], i.e.,

$$f_h = m_t\ddot{x}_t + b_t\dot{x}_t + k_t x_t + \alpha_f f_e \quad (44)$$
$$x_t = x_m = \alpha_p x_s \quad (45)$$

where $\alpha_f$ and $\alpha_p$ scale the force and position between the master and slave, and $m_t, b_t, k_t$ are mass, damping, and stiffness of the virtual tool, respectively, and $x_t$ is the position of the virtual tool. While in a conventionally transparent system, the operator interacts with the task environment through a rigid dynamicless tool, the modified transparency measures introduce an intervening virtual tool with adjustable mass-spring-damper dynamics. The tool parameters should be selected such that the tool impedance is as low as possible, while sufficient stability margins are maintained. It should be noted that in rigid contact, the modified transparency requirements in (44)–(45) reduce to the original force and position tracking requirements, if $k_t = 0$.

The combined operator/master dynamics in (37) can be written in the state-space form as follows:

$$\dot{X}_m(t) = A_m X_m(t) + B_m f_{\rm cm}(t) + G_m w_m(t)$$
$$y_m(t) = C_m X_m(t) + D_m f_{\rm cm}(t) + H_m w_m(t) + \upsilon_m(t) \quad (46)$$

where $X_m(t) = [x_m(t)\ v_m(t)]^T$ is the state vector, and $y_m(t) = [x_m(t)\ f_h(t)]^T$ is the output vector. The control signal $f_{\rm cm}(t)$ has been introduced in (35), and the disturbance signal is $w_m(t) = [f_h^*(t)\ \tilde{f}_{\rm cm}(t)]^T$, where $\tilde{f}_{\rm cm}(t)$ is the disturbance at the control signal $f_{\rm cm}(t)$; and $\upsilon_m(t)$ is a vector of measurement noise. Similarly, the slave/environment dynamics in (40) and (42) can be written as

$$\dot{X}_s^i(t) = A_s^i X_s^i(t) + B_s^i f_{\rm cs}(t) + G_s^i w_s(t), \quad i = 1,2,3$$
$$y_s^i(t) = C_s^i X_s(t) + D_s^i f_{\rm cs}(t) + H_s^i w_s(t) + \upsilon_s(t) \quad (47)$$

where indices 1, 2, 3 correspond to free motion, contact with a flexible environment, and contact with a rigid environment, respectively; $X_s^{1,2,3}(t) = [x_s(t)\ v_s(t)]^T$; $y_s(t) = [x_s(t)\ f_e(t)]$ is the measurement vector. The control signal is $f_{\rm cs}(t)$, and the disturbance vector is $w_s(t) = [f_e^*(t)\ \tilde{f}_{\rm cs}(t)]^T$. Note that the state-transition matrices are functions of the contact state $i$. The desired tool dynamics in (44) can also be written as

$$\dot{X}_t(t) = A_t X_t(t) + B_t u_t(t)$$
$$y_t(t) = X_t(t) \quad (48)$$

where $X_t(t) = [x_t(t)\ v_t(t)]^T$, $u_t(t) = [f_h(t)\ f_e(t)]^T$.

The change in the slave/environment dynamics due to rigid contact, and parameter variations due to flexible contact, can be handled with a multimodel control approach, in which mode-based controllers are designed for different phases of the operation [41], [42]. In this strategy, a controller is designed for free motion; another controller handles flexible contacts, while a third controller is employed for interacting with rigid environments. Alternatively, it is possible to design a single controller that can function for both free motion and flexible contact at the expense of a more conservative design.

### A. Free Motion/Soft Contact

The states of the system for the cases of free motion/soft contact are defined as follows:

$$X(t) = [\alpha_p X_s(t) - X_m(t) \quad X_m(t) - X_t(t) \quad X_t(t)]^T \quad (49)$$

where $X_m(t), X_s(t)$, and $X_t(t)$ have been introduced in (46), (47), and (48); and $\alpha_p$ has been defined in (44) and (45). The above choice of states facilitates the application of the LQG method by including the tracking errors of interest into the state vector. The evolution of the states is governed by

$$\dot{X}(t) = AX(t) + Bu(t) + Gw(t)$$
$$u(t) = [f_{\rm cm}(t) \quad f_{\rm cs}(t-\tau_1)]^T$$
$$w(t) = [f_h^*(t) \quad f_e^*(t) \quad \tilde{f}_{\rm cm}(t) \quad \tilde{f}_{\rm cs}(t)]^T. \quad (50)$$

It is straightforward to obtain the system matrices $A, B, G$ from $A_m, B_m, C_m, D_m, G_m, H_m, A_s, B_s, C_s,\ D_s, G_s, H_s, A_t$, and $B_t$. The measurement vector is

$$y(t) = [y_m(t) \quad y_s(t-\tau_2) \quad y_t(t-\tau_2)]^T. \quad (51)$$

These observations are the actual sensor readings $x_m(t)$, $f_h(t), x_s(t)$, and $f_e(t)$, as well as the virtual intervening tool states from (48).

Throughout the rest of the paper, we assume that the teleoperation controller is located at the master side, with the forward and return communication delays being $\tau_1$ and $\tau_2$, respectively. Therefore, the slave control signal and measurement are delayed by $\tau_1$ and $\tau_2$, respectively. The virtual tool observations, $x_t(t-\tau_2)$ and $v_t(t-\tau_2)$ which are produced by the control algorithm, are also delayed, since they depend on the environment force $f_e(t-\tau_2)$ that is transmitted from the slave to the master site.

The operator's exogenous force $f_h^*(t)$ is part of the unknown disturbance vector $w(t)$ that excites the teleoperation control system and produces output error. In the LQG control-design framework, the disturbance is modeled as a stochastic signal, often a white Gaussian noise, and the cost function in (18) is minimized accordingly. In the frequency domain, this can be interpreted as minimizing the area under mixed weighted power spectrums of the output errors and the control signals. White noise has a flat power spectrum and excites the system at all frequencies equally. Using such a model is equivalent to assuming minimum knowledge about the input disturbance [43]. However, it is reasonable to assume that the operator exogenous force has a lowpass power spectrum, as the user cannot apply high-frequency intentional forces to the master device. This rather imprecise knowledge about the exogenous force can be incorporated into the LQG framework using the following simple stochastic model for the exogenous force with two poles at $-\alpha_{fh}$:

$$\ddot{f}_h^*(t)+2\alpha_{fh}\dot{f}_h^*(t)+\alpha_{fh}^2 f_h^*(t)=n_f(t) \tag{52}$$

where $n_f(t)$ is a white Gaussian noise. While the proposed model has not been validated by human factors studies, our experience shows that in practice, it can significantly enhance the performance of the LQG-based teleoperation controller compared with a white-noise model. This should not be surprising, as using such model causes the controller to minimize the cost function in (18) in the frequency range where operator force has most of its energy. In [44], a similar approach has been successfully used by the first author for the cancellation of biodynamic feedthrough in joystick-controlled machines.

The state-space equations of the system in free motion/soft contact after the augmentation of $f_h^*$ into the state vector are given by

$$\begin{aligned}\dot{X}_f(t)&=A_fX_f(t)+B_fu_f(t)+G_fw_f(t)\\ y_f(t)&=C_fX_f(t)+H_fw_f(t)+v_f(t)\end{aligned} \tag{53}$$

with

$$\begin{aligned}X_f(t)&=[X(t)\quad f_h^*(t)\quad \dot{f}_h^*(t)]^T\\ y_f(t)&=y(t)=[y_m(t)\quad y_s(t-\tau_2)\quad y_t(t-\tau_2)]^T\\ u_f(t)&=u(t)=[f_{\rm cm}(t)\quad f_{\rm cs}(t-\tau_1)]^T\\ w_f(t)&=[n_f(t)\quad f_e^*(t)\quad \tilde{f}_{\rm cm}(t)\quad \tilde{f}_{\rm cs}(t)]^T\\ v_f(t)&=[v_m(t)\quad v_s(t)\quad 0]^T.\end{aligned} \tag{54}$$

Assuming that the master, slave, and tool measurements are the first, second, and third output channels and master, and slave control signals are the first and second input channels, respectively, then $d_I^1=d_O^1=0, d_I^2=\tau_1, d_O^2=\tau_2, d_O^3=\tau_2$. Also, the maximum output delay is $d_O^m=\tau_2$, and therefore, $h_1^m=\tau_2, h_2^m=\tau_1+\tau_2$. After the application of the transformations in (6) and (16), the reduced system dynamics in free motion/soft contact are governed by the following equations:

$$\begin{aligned}\dot{Z}_f(t)&=A_{zf}Z_f(t)+B_{zf}u_z(t)+G_{zf}w_f\,(t-d_O^m)\\ y_{zf}(t)&=C_{zf}Z_f(t)+v_{zf}(t).\end{aligned} \tag{55}$$

### B. Rigid Contact

When the slave is in rigid contact, its linearized dynamics are governed by (42)–(43). In this case, the vector of states including the master and slave subsystems is chosen as

$$\begin{aligned}X(t)=[x_m(t)-\alpha_p x_s(t)\quad v_m(t)\quad x_s(t)\quad \tilde{f}_e(t)\\ \alpha_f\tilde{f}_e(t)-\tilde{f}_h(t)]^T\end{aligned} \tag{56}$$

and the measurement vector is

$$y(t)=[y_m(t)\quad x_s(t-\tau_2)\quad \tilde{f}_e(t-\tau_2)]^T. \tag{57}$$

In (56), $\tilde{f}_e(t)$ and $\tilde{f}_h(t)$ are generated by passing force-sensor measurements $f_e(t)$ and $f_h(t)$ through a first-order filter with pole at $-\beta$, i.e.,

$$\dot{\tilde{f}}_e(t)+\beta\tilde{f}_e(t)=\beta f_e,\quad \dot{\tilde{f}}_h(t)+\beta\tilde{f}_h(t)=\beta f_h. \tag{58}$$

The new state $\tilde{f}_e$ is added to system to handle the algebraic constraint in (42)–(43). The first-order filters introduce new states for the slave and enable a routine application of the LQG control synthesis. The dynamics of the filtered force-tracking error $\alpha_f\tilde{f}_e-\tilde{f}_h$ can be easily derived from the filter equations above. The slave position in rigid contact, $x_s(t)$, is modeled by

$$\dot{x}_s(t)=w_{xs}(t) \tag{59}$$

where $w_{xs}(t)$ is a low-power white Gaussian noise. The steps for incorporating the operator's exogenous force $f_h^*(t)$ into the system states are similar to those in the previous case, and will not be repeated here. The dynamics of the augmented system can be expressed by the following equations:

$$\begin{aligned}\dot{X}_r(t)&=A_rX_r(t)+B_ru_r(t)+G_rw_r(t)\\ y_r(t)&=C_rX_r(t)+D_ru_r(t)+H_rw_r(t)+v_r(t)\end{aligned} \tag{60}$$

with

$$\begin{aligned}X_r(t)&=[X(t)\quad f_h^*(t)\quad \dot{f}_h^*(t)]^T\\ y_r(t)&=y(t)=[y_m(t)\quad x_s(t-\tau_2)\quad \tilde{f}_e(t-\tau_2)]\\ u_r(t)&=[f_{\rm cm}(t)\quad f_{\rm cs}(t-\tau_1)]^T\\ w_r(t)&=[n_f(t)\quad \tilde{f}_{\rm cm}(t)\quad \tilde{f}_{\rm cs}(t)\quad w_{xs}(t)]\\ v_r(t)&=[v_m(t)\quad 0].\end{aligned} \tag{61}$$

It should be noted that the virtual tool dynamics are not used in the rigid contact controller. Assuming that master and slave inputs and outputs are the first and second channels, respectively, then $d_I^1=d_O^1=0, d_I^2=\tau_1, d_O^2=\tau_2$. The maximum output

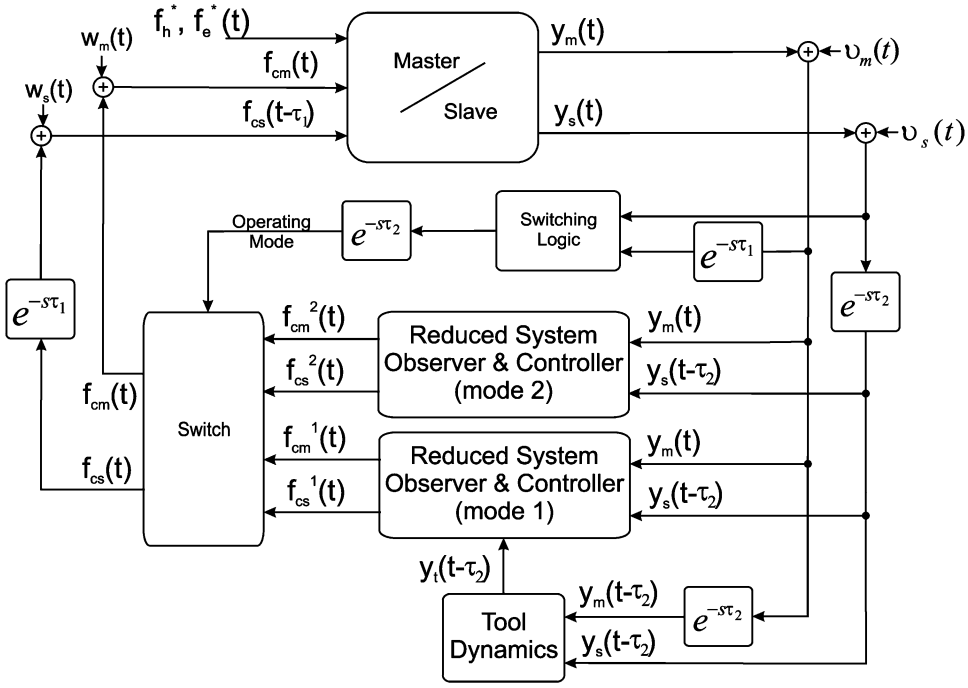


Fig. 3. Teleoperation system with controller at master side.

delay is $d_O^m = \tau_2$ and hence, $h_1^m = \tau_2, h_2^m = \tau_1 + \tau_2$. After the application of the state and measurement transformations, the dynamics of the reduced system are governed by

$$\begin{aligned} \dot{Z}_r(t) &= A_{zr}Z_r(t) + B_{zr}u_z(t) + G_{zr}w_r\,(t - d_O^m) \\ y_{zr}(t) &= C_{zr}Z_r(t) + \upsilon_{zr}(t). \end{aligned} \tag{62}$$

To achieve the teleoperation performance objectives, the $Q$ and $R$ matrices for free motion/soft contact are selected as

$$X_f(t)^T Q_f X_f(t) = q_1(\alpha_p x_s(t) - x_m(t))^2 + q_2(x_m(t) - x_t(t))^2 \tag{63}$$

with $q_1 > 0$ and $q_2 > 0$. Similarly, for rigid contact

$$X_r(t)^T Q_r X_r(t) = q_1(x_m(t) - \alpha_p x_s(t))^2 + q_2(\alpha_f \tilde{f}_e(t) - \tilde{f}_h(t))^2. \tag{64}$$

The quadratic terms in (63) and (64) involve position and force tracking errors at concurrent sample times. Therefore, despite the presence of $\tau_1 + \tau_2$ seconds round-trip delay, the controller attempts to produce nondelayed position and force tracking, as well as tool impedance shaping. Also, the matrices $Q_f$ and $Q_r$ are positive semidefinite as opposed to positive definite. This is critical for the design of the teleoperation controller, since the system must be allowed to move freely. Therefore, only the tracking errors of interest are penalized in (18), and the gains corresponding to the rest of the states in the $Q$'s are set to zero. The LQG control synthesis in (18) is conducted using the transformed states $Z(t)$ rather than the original states. Note that

$$\begin{aligned} &e^{-Ad_o^m} X(t) \\ &\quad = X(t - d_o^m) + \sum_{j=1}^{n_I} \int_{t-h_j^m}^{t-d_I^j} e^{A(t-s-h_j^m)} B_j u_j(s) ds \approx Z(t). \end{aligned} \tag{65}$$

Therefore, proper scaling for matrices $Q_f$ and $Q_r$ may be obtained by considering

$$X(t)^T Q X(t) \approx Z(t)^T e^{A^T d_o^m} Q e^{Ad_o^m} Z(t). \tag{66}$$

The schematic of the proposed multimodel LQG teleoperation control system is displayed in Fig. 3. The sensor measurements are the master and slave positions, as well as the hand and environment forces. Delayed hand and environment force signals are used to generate delayed virtual tool position and velocity. These synthesized observations, along with the actual observations, enter mode-based LQG controller blocks at the master site which produce mode-based control signals. The switching logic, located at the slave side, uses the sensor measurements to identify the mode of operation and sends the result back to the controller at master side. This information is used in selecting the pair of control signals to be transmitted to the master and slave actuators.

The disturbances $f_h^*(t)$ and $f_e^*(t)$ are the cause of motion in teleoperation. The LQG design framework attempts to minimize the effect of these stochastic perturbations on the tracking errors, and as such, coordinates the master and slave robots. For example, in free motion/soft contact, the disturbances drive the virtual tool dynamics in (48), which are not controllable by the control signals. Therefore, the controller must move the master and slave in response to operator's exogenous force such that the transparency objectives are achieved, i.e., the tracking errors among master, slave, and tool are minimized.

Nominal model parameters of the operator, master robot, slave robot, and environment dynamics are used by the mode-based controllers. While the adaptive nonlinear controller in (28)–(30) renders the master and slave parameters constant, the operator and environment dynamics are usually unknown and time-varying. Any deviation from the nominal

TABLE I
SYSTEM AND CONTROLLER PARAMETERS

| System Parameters | | | |
|---|---|---|---|
| Master | $m_m = 3.5$ kg $b_m = 2.2$ N.s/m $k_m = 0$ N/m | Arm | $m_h = 2.0$ kg $b_h = 1$ N.s/m $k_h = 60.0$ N/m |
| Slave | $m_s = 3.5$ kg $b_s = 1.6$ N.s/m $k_s = 0$ N/m | Environment | $m_e = 0$ kg $b_e = 0$ N.s/m $k_e = 0$ N/m |
| Virtual Tool | $m_t = 3.0$ kg $b_t = 1.0$ N.s/m $k_t = 0$ N/m | Other | $\alpha_f = 1$ $\alpha_p = 1$ $\alpha_{fh} = 0.01$ rad/s $\beta = 0.8$ rad/s |
| LQG Controller Parameters | | | |
| Free Motion | | Rigid Contact | |
| $q_1 = q_2 = 4 \times 10^5$ m$^{-2}$<br>$R = \text{diag}\,(0.1\ \text{N}^{-2}, 0.1\ \text{N}^{-2})$<br>$E\{w_f w_f^T\} = \text{diag}\,(10^4\ \text{N}^2/\text{s}^4, 200\ \text{N}^2, 10^{-3}\ \text{N}^2, 10^{-3}\ \text{N}^2)$ | | $q_1 = 10^5$ m$^{-2}$ $q_2 = 50$ N$^{-2}$<br>$R = \text{diag}\,(0.01\ \text{N}^{-2}, 0.01\ \text{N}^{-2})$<br>$E\{w_r w_r^T\} = diag\,(1\ \text{N}^2/\text{s}^4, 10^{-6}\ \text{N}^2, 10^{-6}\ \text{N}^2, 10^{-5}\ \text{m}^2/\text{s}^2)$ | |

parameters can degrade the system performance and even cause instability. Tightening the control loops through the adjustment of the LQ controller parameters could improve performance by reducing the tracking errors and increasing the speed of the system response. However, this would be achieved at the expense of reduced stability margins and potential instability due to parametric uncertainty.

The stability of switching is a cause of concern in the proposed method. In our experience, a careful selection of the switching strategy will usually provide a stable contact-transition behavior. While the stability of mode-based controllers is guaranteed by the LQG design, it is difficult to prove the stability of the switched teleoperation control system. This remains beyond the scope of this paper, and will be a subject of future research. The interested reader is referred to [45] for stability analysis of a gain-switching teleoperation controller. Finally, the proposed method requires estimation of forward and return communication time delays. This can be easily obtained if the delays in both directions are equal, otherwise, the master and slave computers' clocks can be synchronized to an external universal time reference, e.g., Universal Coordinated Time, via GPS or special radio signals [46]. Once the computer clocks are synchronized, the data packets can be time-stamped for delay estimation. The proposed teleoperation controller can also be employed under a time-varying delay by introducing buffers that can store the time-stamped measurement and control signals and add artificial latency to render the delay to a constant value determined by its maximum.

## V. CONTROL DESIGN AND ROBUST STABILITY ANALYSIS FOR SINGLE-AXIS TELEOPERATION

The proposed multimodel LQG control scheme is applied to a linear single-axis bilateral teleoperation system involving two similar masses. Since the master and slave dynamics are already linear and known, the adaptive nonlinear impedance controller is not needed for this example. The controller is implemented at the master side, and the forward and return communication delays are assumed equal, i.e., $\tau_1 = \tau_2 = \tau$. Throughout the rest of this paper, the delay values correspond to a round-trip communication unless otherwise noted.

The operator manipulates the slave robot in free motion and in contact with a rigid environment. Two different controllers are designed; the first controller is intended for free-motion operation, while a second controller is designed for rigid contact. The system parameters, which reflect those of the experimental setup in the next section, are given in Table I. Typical values have been chosen for the arm mass, damping, and stiffness. The LQG control parameters are also presented in this table. The values of measurement and disturbance noise powers were initially selected based on sensor and actuator specifications, as well as a typical level of operator hand force, and later refined based on simulation and experimental results. The $Q$ and $R$ in the LQG synthesis play a pivotal role in the tradeoff between performance and stability. A large $Q$ and small $R$ would generally yield faster poles, small tracking errors, and enhanced performance at the expense of reduced robustness. We have manually tuned these parameters to achieve a balance between these requirements.

The robustness of the proposed controller w.r.t. parametric uncertainty can be investigated using classical linear analysis tools such as the Nyquist theorem. Among the model parameters, those of environment and operator are subject to uncertainty, whereas the master and slave parameters are known because of the use of the adaptive nonlinear impedance controller in (28)–(30). In Fig. 4, the robustness of the mode-based controllers w.r.t. variations in individual parameters and as a function of communication latency is examined. The environment stiffness in the design of the free-motion controller is set to 0 N/m. The robustness of this controller w.r.t. uncertainty in the environment stiffness is examined in Fig. 4(a), where the maximum stiffness for stability decreases by the amount of time delay from more than 13 000 N/m for round-trip delays less than 20 ms to about 310 N/m for a delay of 250 ms.

In Fig. 4(b) and (d), the sensitivity of the free-motion and rigid-contact controllers w.r.t. variations in the operator's arm mass are examined, where the nominal value of the arm mass used in the design is 2.0 kg according to Table I. By a comparison of these figures, it is evident that the free-motion controller is more robust w.r.t. the arm mass uncertainty than the rigid-contact controller. Nevertheless, both controllers demonstrate good stability margins w.r.t. such uncertainty. Again, the stability margins reduce as the time delay increases.

In Fig. 4(c), the robustness of the free-motion controller w.r.t. uncertainty in the operator's arm stiffness is demonstrated. The nominal value of stiffness used in the controller design is 60 N/m. Interestingly, the gain margin trend w.r.t. the time delay is slightly different in this case, as it first increases to a maximum value around 70 ms and then drops off after this point.

The robust stability analysis was also performed for simultaneous variations in two system parameters at a fixed delay of 125 ms, the results of which are given in Fig. 5. To obtain these graphs, one parameter was varied in fixed-size steps, while the stability bound on the second parameter was computed using

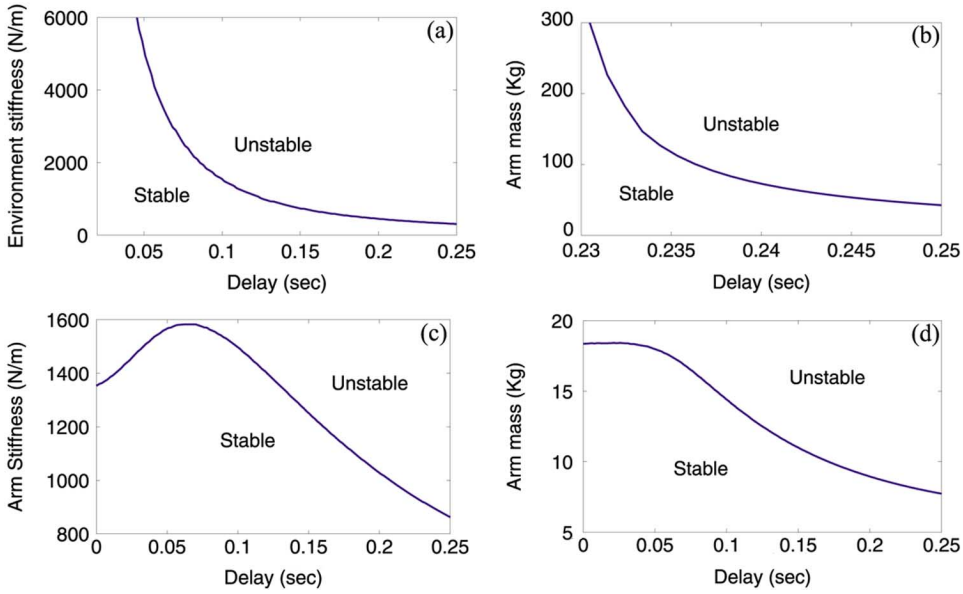


Fig. 4. Robustness of mode-based controllers as a function of delay w.r.t. mismatches in model parameters. (a), (b), (c) Free-motion controller. (d) Rigid-contact controller.

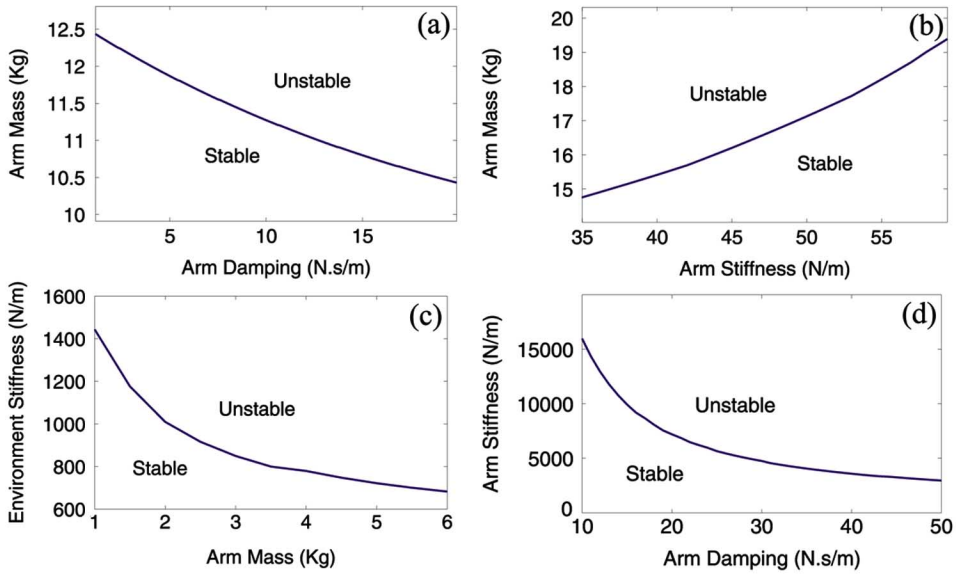


Fig. 5. Robustness w.r.t. simultaneous changes in two parameters for a delay of 125 ms. (a), (b), (d) Rigid-contact controller. (c) Free-motion controller.

the Nyquist criterion. From the above analysis, as well as the experimental results that will be presented later in the paper, it can be concluded the mode-based controllers are reasonably robust w.r.t. the type of uncertainties considered in the analysis for round-trip delays up to 250 ms. Obviously, it is difficult to specify objective targets for the controller robustness margins. The designer should set the performance and robustness goals based on the application requirements, and then tune the controller design parameters to achieve those objectives, if possible.

## VI. Experimental Results

Fig. 6 depicts the single-axis teleoperation experimental setup used in this paper. Designed and manufactured by Quanser, this device consists of two linear carts powered by DC motors employed as master (right) and slave (left). The middle cart is clamped to the track and is used as a rigid wall. The angular movements of the motor shafts are transformed to linear movement using a rack and pinion mechanism. The motors are equipped with optical encoders that produce 4096 pulses per revolution. This yields a linear position measurement resolution of $9.74 \times 10^{-6}$ m. The Coulomb friction of the carts are compensated by active control. Master and slave carts are equipped with ATI Mini40 force sensors that measure the operator and environment forces. The control system runs on a PC platform using the *Tornado/VxWorks* realtime operating system, and is interfaced to the hardware by a $Q8$ data acquisition board from Quanser. The control code is implemented by the *Matlab Real-time Workshop* toolbox.

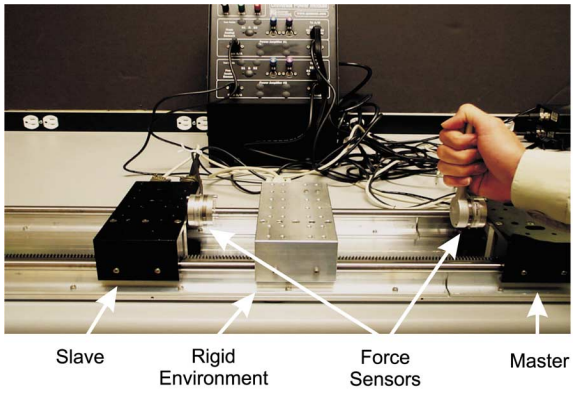


Fig. 6. Experimental setup.

The *ode1 (Euler)* integration routine of Matlab/Simulink is used for the discrete-time implementation of the proposed continuous-time controller. This routine is applied to the linear dynamics in (17) for the calculation of the transformed measurement vector and the Kalman filter dynamics in (21). The old values of the control signal needed in (17) are stored in a buffer of appropriate size. The control update rate is set to 1024 Hz, which is much higher than a typical closed-loop bandwidth of the teleoperation control system. Therefore, a discrete approximation of the continuous-time controller should be valid for practical purposes.

*Controller Switching:* The switching logic used in this paper is rather simple. While in free motion, the controller enters the rigid mode if the magnitude of the measured environment force surpasses a predefined threshold. This will ensure that the force-measurement noise cannot trigger a unintended switching event. To return to the free-motion mode, the average slave velocity over a short window of time and the operator's measured force in the direction away from the contact must be below and above small predefined thresholds. Such logic will eliminate the possibility of erroneous switching due to the bouncing against the rigid environment during the transition period. Also, the number of free-to-rigid bounces may be reduced simply by adding extra damping to the slave controller during the transition period. While in rigid contact, the virtual-tool dynamics in Fig. 3 is disabled and the tool position is reset to the slave position. This will enable a smooth transition from rigid contact to free motion.

The experiments were conducted using the parameters in Table I and for three different round-trip time delays, i.e., 63, 125, and 250 ms. The communication latency was emulated by adding buffers of appropriate size that store and delay the slave measurements and control actions. To enable comparison between the proposed controller and a standard teleoperation method, the results of experiment with a four-channel teleoperation controller are also reported.

### A. LQG Controller With 63 ms Delay

In Fig. 7, the responses of the proposed controller under 63 ms of communication delay are plotted. The system is initially at rest until roughly $t = 0.5$ s when the operator begins moving the master/slave units in free motion. In this phase of operation, the operator should only feel the dynamics of the virtual tool. The nonzero hand force observed in the free-motion portions of Fig. 7 is due to these dynamics. The positions of master, slave,

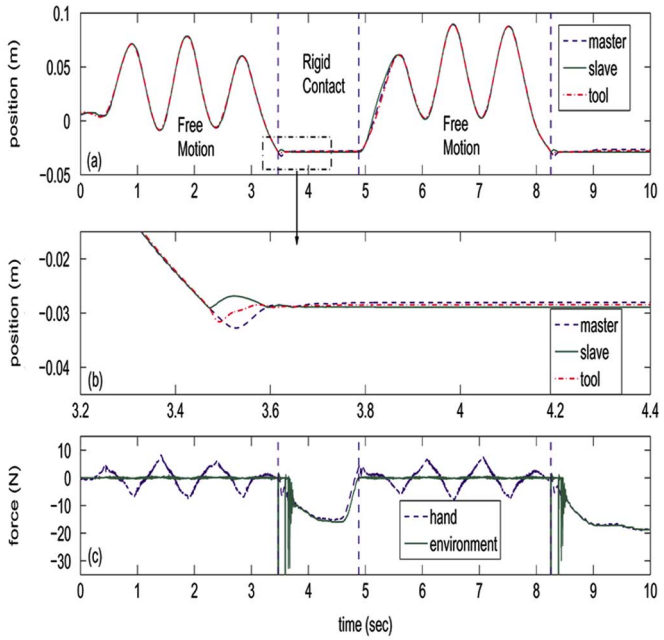


Fig. 7. LQG controller with 63 ms delay in experiment. (a) Position tracking for master/slave/virtual tool. (b) Contact transition. (c) Force tracking.

and virtual tool closely follow each other in free motion, which confirm that the performance objectives in (44) and (45) are both achieved with very high precision.

At $t \simeq 3.5$ s, the slave makes an initial contact with the rigid wall. This causes the controller to switch to the rigid mode after approximately 32 ms, the time that is required for the environment force measurement to arrive at the controller at the master side. There is about a 0.1 s transition period before the contact becomes stable, during which two bounces occur against the wall. The switching logic enforces the rigid-mode controller over this time. At the operator's end and upon the initial contact, there is a position-tracking error which may increase by the amount of time delay and the master speed at the time of initial contact. This can be explained by the inability of the controller to predict an abrupt change in the environment characteristic from free motion to rigid contact. Nevertheless, the error is quickly reduced to a very small constant value by the controller. This small tracking error under rigid contact slightly increases by the amount of delay, as will be seen later in the paper. The resulting transient response was found acceptable by the operator in this case, as well as the two other following cases with longer delays.

During the course of the first rigid contact from time 3.5–5 s, the environment and hand forces as well as the master and slave positions closely track each other, as can be seen in Fig. 7. The contact is stable and is perceived rigid by the operator, as is evident by the constant master position, despite the changes in the hand force. At $t \simeq 5$ s, the operator withdraws the master, and consequently, the master/slave system returns to free motion following a smooth transition. Finally, a second rigid contact occurs at $t \simeq 8.2$ s.

### B. LQG Controller With 125 ms Delay

Fig. 8 illustrates that the responses of the controller for a round-trip delay of 125 ms. As in the previous case, the ex-

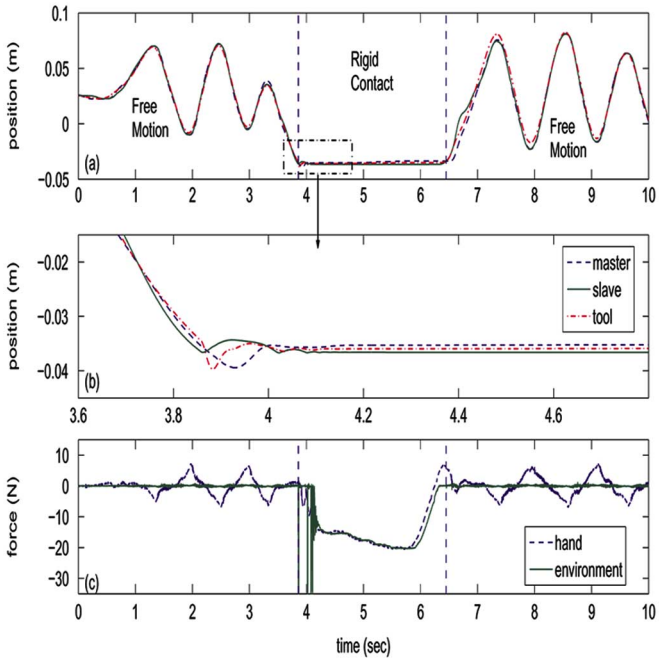


Fig. 8. LQG controller with 125 ms delay in experiment. (a) Position tracking for master/slave/virtual tool. (b) Contact transition. (c) Force tracking.

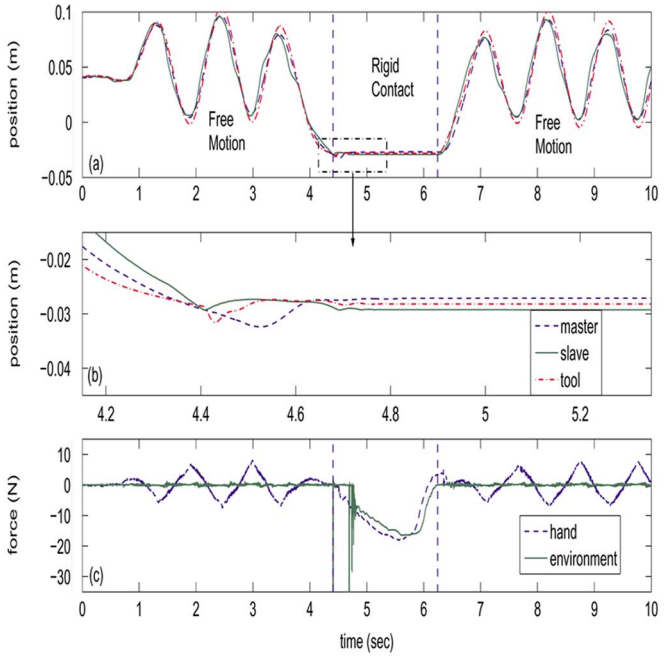


Fig. 9. LQG controller with 250 ms delay in experiment. (a) Position tracking for master/slave/virtual tool. (b) Contact transition. (c) Force tracking.

periments starts with the master/slave at rest, followed by a free-motion operation and subsequent rigid-contact and free-motion phases. The transitions from free motion to rigid contact and *vice versa* are stable. Three bounces happen during the free-to-contact transition period which is about 0.25 s, slightly longer than that of the previous case. The position tracking and virtual tool rendering in free motion as well as position and force tracking in rigid contact are quite satisfactory.

### C. LQG Controller With 250 ms Delay

In Fig. 9, the results of an experiment with the proposed teleoperation controller under 250 ms of communication latency are presented. Once again, the mode transitions are stable with three bounces against the wall, although the free-to-rigid transient time has increased to about 0.35 s in this case. The initial position-tracking error during transition from free motion to rigid contact has also slightly increased. Despite slight degradation in the performance of the free-motion tracking, the results are still satisfactory.

### D. Four-Channel Controller With 250 ms Delay

A standard four-channel [3] teleoperation controller was also implemented on our experimental setup. The controller includes feedforward force gains, as well as a spring-damper-type position coupler between the master and slave units. The controller employs the same sensor observations as those in the multimodel LQG controller, and therefore, provides a basis for comparison. In the case of identical master and slave, a transparent response can be achieved with unit feedforward force gains along with a spring-damper coupling for position-drift compensation. However, delay-induced instability can limit the amount of the force gains. In our experimental setup, we were able to increase the gains up to 0.4 while maintaining a stable response under a round-trip delay of 250 ms. The coupling stiffness and damping were set to 250 N/m and 5 Ns/m, respectively. The operator's perceived impedance is also a limiting factor in the selection of the controller gains. While increasing the damping could improve stability, at the same time, it can make the system sluggish, and therefore interfere with the operator's perception of the environment.

The position and force tracking responses of the four-channel controller are displayed in Fig. 10. A large position-tracking error is observed both in free motion and rigid contact compared with that of the LQG controller in Fig. 9. The rigid contact is perceived relatively soft by the operator as the feedforward-force gains are substantially less than one, for maintaining the stability. In addition to its large tracking errors, and perhaps even more critical, the four-channel teleoperation controller demonstrates a highly sluggish response, compared with that of the LQG controller. This can be observed by comparing the level of the operator's force effort for comparable master/slave displacements in free motion in Figs. 9 and 10.

In Table II, the root mean square (RMS) tracking errors of the LQG controller at different delay levels and that of the four-channel teleoperation controller are compared. It is clear that the proposed controller demonstrates very good performance at all three levels of the delay and outperforms the four-channel controller. It should be emphasized that the critical difference in the perceived tool impedances that exist between the LQG and four-channel approaches cannot be observed from data presented in this table.

## VII. Conclusions and Future Work

Most existing teleoperation control techniques sacrifice transparency objectives in order to gain robust stability in the presence of communication delay between the master and

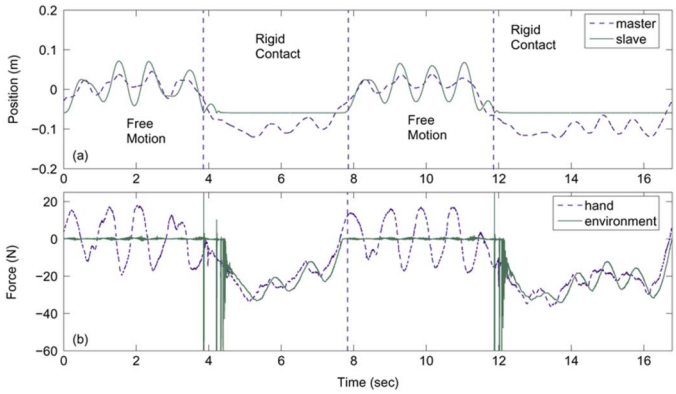


Fig. 10. Four-channel controller with 250 ms delay in experiment. (a) Position tracking. (b) Force tracking.

TABLE II
RMS TRACKING ERRORS IN EXPERIMENTS

| Controller/delay | $\frac{RMS(x_m - x_s)}{peak\text{-}peak}$ | $\frac{RMS(x_m - x_f)}{peak\text{-}peak}$ | $\frac{RMS(f_h - f_e)}{peak\text{-}peak}$ |
|---|---|---|---|
| LQG/ 63 ms | 1.37% | 1.10% | 3.81% |
| LQG/ 125 ms | 2.64% | 2.48% | 6.90% |
| LQG/ 250 ms | 4.2% | 3.82% | 14.75% |
| 4-channel/ 250 ms | 18.18% | - | 23.41% |

slave sites. With the aim of improving transparency, we studied the problem of bilateral teleoperation control under known constant communication delay. A reduction method was proposed to transform a dynamical system with delays in control and measurement channels to a delay-free system suitable for output-feedback control. Teleoperation performance objectives such as nondelayed virtual-tool impedance shaping, position tracking, and force tracking were achieved through multimodel LQG control synthesis using delay-free dynamics. The controller sensitivity to some of the model parameters was examined via the Nyquist analysis. Experiments with a single-axis teleoperation system demonstrated that the proposed approach is highly successful in providing a stable transparent response under round-trip communication delays up to 250 ms, when compared with a conventional four-channel controller.

In order to operate under large delays, based on our experience and results of analysis, a good knowledge of the model parameters is required. This might have been expected, as the proposed method is essentially a model-based predictive controller. In general, it is hard to find a meaningful bound on the time delay that our approach can handle, as such a limit would depend on various factors such as the system dynamics, the required level of performance, and the amount of uncertainty in the parameters. The analytical and experimental results indicated that a good tradeoff between performance and stability margins can be obtained for round-trip delays of up to 200–300 ms in our experimental setup. To move beyond this level, the performance has to be sacrificed in favor of the robust stability of the system.

We are currently developing a decentralized variant of the controller in order to improve its robustness w.r.t. parametric uncertainty. In future, a formal analysis of the stability of the proposed switching control strategy will be performed. Adaptive control for coping with variations in the operator and environment dynamics will also be a subject of future research.

## APPENDIX
## PROOF OF *Theorem 2.1*

### A. Stabilizability

The controllability matrix of the original system with pair $(A, B)$ can be written as

$$\begin{aligned} U &= [B\ AB\ A^2B \cdots A^{n-1}B] \\ &= [B_1 \cdots B_{n_I} | AB_1 \cdots AB_{n_I} | \cdots | A^{n-1}B_1 \cdots A^{n-1}B_{n_I}] \end{aligned} \tag{67}$$

where the rank of $U$ is $\rho(U) = n_c \leq n$. Using the canonical decomposition theorem [35], there exists a state transformation $\bar{X} = PX$, which converts the pair $(A, B)$ to $(\bar{A}, \bar{B})$

$$\bar{A} = PAP^{-1} = \begin{bmatrix} \bar{A}^c & \bar{A}^{12} \\ 0 & \bar{A}^{\bar{c}} \end{bmatrix}, \quad \bar{B} = PB = \begin{bmatrix} \bar{B}^c \\ 0 \end{bmatrix} \tag{68}$$

such that the pair $(\bar{A}^c, \bar{B}^c)$ is controllable. The state transformation matrix $P$ is defined as

$$P^{-1} \triangleq Q = [q_1 \cdots q_{n_c} \cdots q_n] \tag{69}$$

where $q_1 \cdots q_{nc}$ are $n_c$ linearly independent columns of matrix $U$, and the last $n - n_c$ columns are arbitrarily chosen vectors that make the matrix $Q$ nonsingular. Since the original system is assumed stabilizable, $\bar{A}^c$ would contain all unstable modes, if any.

From (8), the controllability matrix of the transformed system represented by the pair $(A_z, B_z)$ is given by

$$\begin{aligned} U_z &= \left[B_z\ A_zB_z\ A_z^2B_z \cdots A_z^{n-1}B_z\right] \\ &= \left[e^{-Ah_1^m}B_1 \cdots e^{-Ah_{n_I}^m}B_{n_I} \middle|\ e^{-Ah_1^m}AB_1 \cdots e^{-Ah_{n_I}^m}AB_{n_I} \middle| \cdots \right. \\ &\quad \left. \middle| e^{-Ah_1^m}A^{n-1}B_1 \cdots e^{-Ah_{n_I}^m}A^{n-1}B_{n_I} \right] \end{aligned} \tag{70}$$

where the commutability of matrices $A$ and $e^{-Ah}$ has been used. The following lemma is needed to continue the proof.

*Lemma A.1:* $\rho(U_z) = \rho(U)$.

*Proof:* Reordering the columns of a matrix will not alter its rank, so from (70)

$$\begin{aligned} \rho(U_z) = \rho\Big(\Big[e^{-Ah_1^m}[B_1AB_1 \cdots A^{n-1}B_1] \Big| \cdots \\ \Big| e^{-Ah_{n_I}^m}[B_{n_I}AB_{n_I} \cdots A^{n-1}B_{n_I}]\Big]\Big). \end{aligned} \tag{71}$$

Note that since $e^{-Ah_j^m}$ is a full-rank square matrix, for each $j$

$$\begin{aligned} \rho\Big(\Big[e^{-Ah_j^m}[B_j\ AB_j \cdots A^{n_I-1}B_j]\Big]\Big) \\ = \rho([B_jAB_j \cdots A^{n_I-1}B_j]). \end{aligned} \tag{72}$$

To proceed, we use the Caley–Hamilton theorem, which states that each matrix satisfies its own characteristic polynomial, and therefore, all powers of $A$ greater than or equal to $n$ can be written as a linear combination of $A^k$, for $k < n$ [35]. Using this theorem and the Taylor expansion of $e^{-Ah_j^m}$, one can write

$$e^{-Ah_j^m} = c_0I + c_1A + c_2A^2 + \cdots + c_{n-1}A^{n-1}. \tag{73}$$

Using (73)

$$\begin{aligned} & e^{-Ah_j^m} A^k B_j \\ & \quad = (c_0 I + c_1 A + c_2 A^2 + \cdots + c_{n-1} A^{n-1}) A^k B_j \\ & \quad = l_0 B_j + l_1 A B_j + l_2 A^2 B_j + \cdots + l_{n-1} A^{n-1} B_j. \quad (74) \end{aligned}$$

Considering (72) and (74), one can conclude that for each $j, [B_j \;\; AB_j \cdots A^{n-1}B_j]$ and $e^{-Ah_j^m}[B_j \;\; AB_j \cdots A^{n-1}B_j]$ span the same space. Therefore, $U$ and $U_z$ are of the same rank and the proof of *Lemma A.1* is complete. Q.E.D.

The canonical form of the reduced system represented by the pair $(\bar{A}_z, \bar{B}_z)$ can be generated using the same transformation $P$ in (69) for the original system, i.e.,

$$\bar{A}_z = P A_z P^{-1}, \quad \bar{B}_z = P B_z, \quad \text{or} \quad P^{-1}\bar{B}_z = B_z. \quad (75)$$

Substituting $A_z$ and $B_z$ from (9) results in

$$\bar{A}_z = PAP^{-1} = \begin{bmatrix} \bar{A}^c & \bar{A}^{12} \\ 0 & \bar{A}^{\bar{c}} \end{bmatrix} \quad (76)$$

$$P^{-1}\left[\bar{b}_z^1 \cdots \bar{b}_z^{n_I}\right] = \left[e^{-Ah_1^m} B_1 \cdots e^{-Ah_{n_I}^m} B_{n_I}\right]. \quad (77)$$

For the $j$th column of (77), one can write

$$P^{-1}\bar{b}_z^j = e^{-Ah_j^m} B_j. \quad (78)$$

Replacing $e^{-Ah_j^m}$ from (73)

$$P^{-1}\bar{b}_z^j = (c_0 I + c_1 A + c_2 A^2 + \cdots + c_{n-1} A^{n-1}) B_j. \quad (79)$$

From the definition of $P^{-1}$ in (69), the first $n_c$ columns of $P^{-1}$ form a basis for the controllability matrix $U$ in (67). Considering (79), the RHS of (77) can be written in terms of the first $n_c$ columns of $P^{-1}$, i.e.,

$$\bar{B}_z = \begin{bmatrix} \bar{B}_z^c \} n_c \\ 0 \end{bmatrix}. \quad (80)$$

Using (76) and (80), the controllability matrix of the pair $(\bar{A}_z, \bar{B}_z)$ can be written as

$$\bar{U}_z = \begin{bmatrix} \bar{B}_z^c & \bar{A}_c \bar{B}_z^c & \cdots & \bar{A}_c^{n-1} \bar{B}_z^c \} n_c \\ 0 & 0 & \cdots & 0 \end{bmatrix}. \quad (81)$$

According to *Lemma A.1*, $\rho(U_z) = \rho(U) = n_c$. Also, since the transformation $P$ is nonsingular, $U_z$ and $\bar{U}_z$ have equal ranks, i.e., $\rho(\bar{U}_z) = n_c$ and consequently, the pair $(\bar{A}^c, \bar{B}_z^c)$ is controllable where $\bar{A}^c$ contains all unstable modes.

### B. Detectability

The proof follows along the same lines as in the case of stabilizability using dual arguments, and will not be presented here for brevity.

## ACKNOWLEDGMENT

The authors would like to thank Wind River Corporation, Alameda, CA, for the donation of Tornado/VxWorks RTOS that was used in this research.

## REFERENCES

[1] C. Melchiorri and A. Eusebi, "Telemanipulation: System aspects and control issues," in *Proc. Model. Cont. Mechan. Robot.*, 1996, pp. 149–183.
[2] R. Taylor and D. Stoianovici, "Medical robotics in computer-integrated surgery," *IEEE Trans. Robot. Autom.*, vol. 19, no. 5, pp. 765–781, Oct. 2003.
[3] D. Lawrence, "Stability and transparency in bilateral teleoperation," *IEEE Trans. Robot. Autom.*, vol. 9, no. 5, pp. 624–637, Oct. 1993.
[4] G. Raju, G. Verghese, and T. Sheridan, "Design issues in 2-port network models of bilateral remote teleoperation," in *Proc. IEEE Int. Conf. Robot. Autom.*, 1989, pp. 1317–1321.
[5] B. Hannaford, "A design framework for teleoperators with kinesthetic feedback," *IEEE Trans. Robot. Autom.*, vol. 5, no. 4, pp. 426–434, Aug. 1989.
[6] G. Leung, B. Francis, and J. Apkarian, "Bilateral controller for teleoperators with time delay via mu-synthesis," *IEEE Trans. Robot. Autom.*, vol. 11, no. 1, pp. 105–116, Feb. 1995.
[7] H. Kazerooni, T. Tsay, and K. Hollerbach, "A controller design framework for telerobotic systems," *IEEE Trans. Control Syst. Technol.*, vol. 1, no. 2, pp. 50–62, Mar. 1993.
[8] Y. Yokokohji and T. Yoshikawa, "Bilateral control of master-slave manipulators for ideal kinesthetic coupling-formulation and experiment," *IEEE Trans. Robot. Autom.*, vol. 10, no. 5, pp. 605–620, Oct. 1994.
[9] J. Colgate, "Robust impedance shaping telemanipulation," *IEEE Trans. Robot. Autom.*, vol. 9, no. 4, pp. 374–384, Aug. 1993.
[10] J. Yan and S. Salcudean, "Teleoperation controller design using H infinity -optimization with application to motion-scaling," *IEEE Trans. Control Syst. Technol.*, vol. 45, no. 3, pp. 244–258, May 1996.
[11] S. Sirouspour, "Modeling and control of cooperative teleoperation systems," *IEEE Trans. Robot.*, vol. 21, no. 6, pp. 1220–1225, Dec. 2005.
[12] W.-H. Zhu and S. Salcudean, "Stability guaranteed teleoperation: An adaptive motion/force control approach," *IEEE Trans. Autom. Control*, vol. 45, no. 11, pp. 1951–1969, Nov. 2000.
[13] D. Lee and P. Li, "Passive bilateral control and tool dynamics rendering for nonlinear mechanical teleoperators," *IEEE Trans. Robot.*, vol. 21, no. 5, pp. 936–951, Oct. 2005.
[14] J. Ryu, D. Kwon, and B. Hannaford, "Stable teleoperation with time-domain passivity control," *IEEE Trans. Robot. Autom.*, vol. 20, no. 2, pp. 365–373, Apr. 2004.
[15] K. Hashtrudi-Zaad and S. Salcudean, "Transparency in time-delayed systems and the effect of local force feedback for transparent teleoperation," *IEEE Trans. Robot. Autom.*, vol. 18, no. 1, pp. 108–114, Feb. 2002.
[16] P. Arcara and C. Melchiorri, "Control schemes for teleoperation with time delay: A comparative study," *Robot. Auton. Syst.*, vol. 38, no. 1, pp. 49–64, 2002.
[17] T. Imaida, "Ground-space bilateral teleoperation of ETS-VII robot arm by direct bilateral coupling under 7-s time delay condition," *IEEE Trans. Robot. Autom.*, vol. 20, no. 3, pp. 499–511, Jun. 2004.
[18] R. Anderson and M. Spong, "Bilateral control of teleoperators with time delay," *IEEE Trans. Autom. Control*, vol. 34, no. 5, pp. 494–501, May 1989.
[19] G. Niemeyer and J.-J. Slotine, "Stable adaptive teleoperation," *IEEE J. Ocean. Eng.*, vol. 16, no. 1, pp. 152–162, Jan. 1991.
[20] G. Niemeyer and J.-J. Slotine, "Towards force-reflecting teleoperation over Internet," in *Proc. IEEE Int. Conf. Robot. Autom.*, 1998, pp. 1909–1915.
[21] J. Ueda and T. Yoshikawa, "Force-reflecting teleoperation with time delay by signal filtering," *IEEE Trans. Robot. Autom.*, vol. 20, no. 3, pp. 613–619, Jun. 2004.
[22] D. Lee and M. Spong, "Passive bilateral teleoperation with constant time delay," *IEEE Trans. Robot.*, vol. 22, no. 2, pp. 269–281, Apr. 2006.
[23] H. Baier, "Transparency and stability of bilateral kinesthetic teleoperation with time-delayed communication," *J. Intell. Robot. Syst.: Theory Applic.*, vol. 40, no. 1, pp. 1–22, 2004.
[24] S. Lee and H. Lee, "Modeling, design, and evaluation of advanced teleoperator control systems with short time delay," *IEEE Trans. Robot. Autom.*, vol. 9, no. 5, pp. 607–623, Oct., 1993.
[25] T. Sheridan, "Space teleoperation through time delay: Review and prognosis," *IEEE Trans. Robot. Autom.*, vol. 9, no. 5, pp. 592–606, Oct., 1993.
[26] G. Hirzinger, J. Heindl, and K. Landzettel, "Predictive and knowledge-based telerobotic control concepts," in *Proc. IEEE Int. Conf. Robot. Autom.*, 1989, pp. 1768–1777.

[27] S. Munir and W. Book, "Internet-based teleoperation using wave variables with prediction," *IEEE/ASME Trans. Mechatron.*, vol. 7, no. 2, pp. 124–133, Mar. 2002.
[28] J. Azorin, O. Reinoso, R. Aracil, and M. Ferre, "Generalized control method by state convergence for teleoperation systems with time delay," *Automatica*, vol. 40, pp. 1575–1582, Sep. 2004.
[29] S. Sirouspour and A. Shahdi, "Discrete-time linear quadratic Gaussian control for teleoperation under communication time delay," *Int. J. Robot. Res.*, vol. 25, pp. 187–202, Feb. 2006.
[30] K. Gu and S. Niculescu, "Survey on recent results in the stability and control of time-delay systems," *J. Dyn. Syst., Meas., Control*, vol. 125, pp. 158–165, 2003.
[31] J. Richard, "Time-delay systems: An overview of some recent advances and open problems," *Automatica*, vol. 39, pp. 1667–1694, 2003.
[32] W. H. Kwon and A. E. Pearson, "Feedback stabilization of linear systems with delayed control," *IEEE Trans. Autom. Control*, vol. AC-25, no. 2, pp. 266–269, Apr. 1980.
[33] Z. Artstein, "Linear systems with delayed controls: A reduction," *IEEE Trans. Autom. Control*, vol. AC-27, no. 4, pp. 869–879, Aug. 1982.
[34] P. Park, Y. Moon, and W. Kwon, "A stabilizing output-feedback linear quadratic control for pure input-delayed systems," *Int. J. Control*, vol. 72, no. 5, pp. 385–391, 1999.
[35] C. T. Chen, *Linear System Theory and Design*. Philadelphia, PA: Saunders, 1984.
[36] G. C. Goodwin, S. F. Graebe, and M. E. Salgado, *Control System Design*. Englewood Cliffs, NJ: Prentice-Hall, 2001.
[37] S. Salcudean, "Control for teleoperation and haptic interfaces," in *Control Problems in Robotics and Automation LNCIS230*, B. Siciliano and K. P. Valavanis, Eds. New York: Springer, 1998, pp. 51–66.
[38] L. Sciavicco and B. Siciliano, *Modeling and Control of Robot Manipulators*. New York: Springer, 2000.
[39] R. Kelly, R. Carelli, M. Amestegui, and R. Ortega, "On adaptive impedance control of robot manipulators," in *Proc. IEEE Int. Conf. Robot. Autom.*, 1989, pp. 572–577.
[40] H. Kazerooni and M. Her, "The dynamics and control of a haptic interface device," *IEEE Trans. Robot. Autom.*, vol. 10, no. 4, pp. 453–464, Aug. 1994.
[41] K. S. Narendra and J. Balakrishnan, "Adaptive control using multiple models," *IEEE Trans. Autom. Control*, vol. 42, no. 2, pp. 171–187, Feb. 1997.
[42] A. Shahdi and S. Sirouspour, "Multiple model control for teleoperation in unknown environments," in *Proc. IEEE Int. Conf. Robot. Autom.*, 2005, pp. 715–720.
[43] M. Athans, "The role and use of stochastic linear-quadratic-Gaussian problem in control system design," *IEEE Trans. Autom. Control*, vol. AC-16, no. 6, pp. 529–552, Dec. 1971.
[44] M. Sirouspour and S. Salcudean, "Suppressing operator-induced oscillations in manual control systems with movable bases," *IEEE Trans. Control Syst. Technol.*, vol. 11, no. 4, pp. 448–459, Jul. 2003.
[45] L. Ni and D. Wang, "A gain-switching control scheme for position-error-based bilateral teleoperation: Contact stability analysis and controller design," *Int. J. Robot. Res.*, vol. 23, no. 3, pp. 255–274, 2004.
[46] D. L. Mills, "Improved algorithms for synchronizing computer network clocks," *IEEE Trans. Netw.*, vol. 3, no. 3, pp. 245–254, Jun. 1995.

**Shahin Sirouspour** (S'00–M'04) was born in Tehran, Iran, in 1973. He received the B.Sc. and M.Sc. degrees in electrical engineering from Sharif University of Technology, Tehran, Iran, in 1995 and 1997, respectively, and the Ph.D. degree in electrical engineering from the University of British Columbia, Vancouver, BC, Canada, in 2003.

He then joined McMaster University, Hamilton, ON, Canada, where he is currently an Assistant Professor in the Department of Electrical and Computer Engineering. His research interests include teleoperation control, haptics, robot-assisted medical intervention, advanced robot controls, machine vision, and medical image processing.

**Ali Shahdi** (S'04) received the B.Sc. degree in electrical engineering from Sharif University of Technology, Tehran, Iran, in 2003, and the M.A.Sc. degree in 2005 from McMaster University, Hamilton, ON, Canada, where he is currently working toward the Ph.D. degree in electrical engineering.

His research interests include teleoperation, haptics, advanced robot controls, and medical robotics.